Laser sintering of thick-film conductors for microelectronic applications

Edward C. Kinzel
School of Mechanical Engineering, Purdue University, West Lafayette, Indiana 47907

Hjalti H. Sigmarsson
School of Electrical and Computer Engineering, Purdue University, West Lafayette, Indiana 47907

Xianfan Xu[a)]
School of Mechanical Engineering, Purdue University, West Lafayette, Indiana 47907

William J. Chappell
School of Electrical and Computer Engineering, Purdue University, West Lafayette, Indiana 47907

(Received 14 August 2006; accepted 28 November 2006; published online 20 March 2007)

This paper investigates fabrication of functional thick metal films using simultaneous laser sintering and patterning along with the fundamental physical phenomena that govern the laser sintering process. The effects of the processing parameters on the quality of the fabricated components are investigated through a heat transfer analysis. We show that our process has potentials for metallization of microelectronics directly onto substrates whose melting temperatures are much lower than the temperature needed for sintering, which is only possible by properly controlling the temperature field during laser sintering. Optimum properties of the fabricated components are obtained when certain thermal conditions are produced during laser heating. © *2007 American Institute of Physics*. [DOI: 10.1063/1.2433711]

I. INTRODUCTION

The conventional process for fabricating thick-film microelectronics is a mature technology. It consists of screen printing a pattern onto a substrate using a process similar to the one used since antiquity for the creation of artwork and decoration. The pattern and substrate are then dried and fired in a high temperature furnace to functionalize the ink. The process is capable of patterning different materials (e.g., conductive, resistive, and dielectric elements) and screen-printable inks have been specifically developed and are commercially available. In addition, the low temperature cofired ceramic (LTCC) approach to packaging allows the fabrication of integrated multilayer circuits with buried passive components. Screen printing can produce feature sizes down to 75 μm; however, the substrate must be capable of withstanding the firing temperature of the ink, which is typically around 850 °C for commonly used ceramic-metal inks.[1] This limits the choice of substrates to materials such as alumina and prevents the use of low temperature and low cost substrates which are ideal for applications such as disposable microelectronic devices such as radio frequency identification (RFID)-type tags and sensors. Polymer based thick-film inks have processing temperatures as low as 120 °C; however, this lower firing temperature comes at the expense of electrical performance.[1] Inks based on metallic nanoparticles have also been demonstrated to have good conductivity at low processing temperatures,[2] although the affordability of these inks is not apparent.

It is desirable to extend the range of possible substrates to include glass and polymers while maintaining the conventional thick-film performance and economy. In addition, increases in operational frequency and interconnect density are generating a demand for quality devices with feature sizes less than 75 μm.[3] Recently, several approaches have been developed to direct write microelectronic devices with mesoscopic feature sizes (10 μm–10 mm) such as ink-jet printing and matrix-assisted pulsed laser evaporation-direct write (MAPLE-DW).[3] Most of these processes provide rapid-prototyping capabilities; however, the patterns deposited by these technologies still require functionalization at high temperatures after deposition. An alternative is using a laser to locally sinter the ink while minimizing the heating of the substrate. Marinov[4] investigated the dc resistance of components fabricated using a combination of deposition of chemical precursors followed by laser sintering. Laser sintering has also been proposed for use with direct write techniques such as MAPLE-DW (Ref. 3) and has been demonstrated with ink-jet printing by Bieri *et al.*[2]

Our recent work[5,6] has demonstrated the viability of using the laser sintering technique to simultaneously pattern and functionalize microcircuits using conventional thick-film inks on substrates with damage thresholds below the firing temperature of the ink. This paper describes a detailed investigation of the process of the laser sintering, particularly the heat transfer process driving the laser sintering and the temperature profile needed for successful sintering of high temperature inks on substrates with low thermal damage thresholds. The finite element method is implemented to numerically simulate the transient temperature profile within the ink layer and the substrate. The effects of the process parameters on the electrical performance of the conductors are identified and correlated with the thermal profiles during laser sintering.

[a)]Author to whom correspondence should be addressed; electronic mail: xxu@ecn.purdue.edu

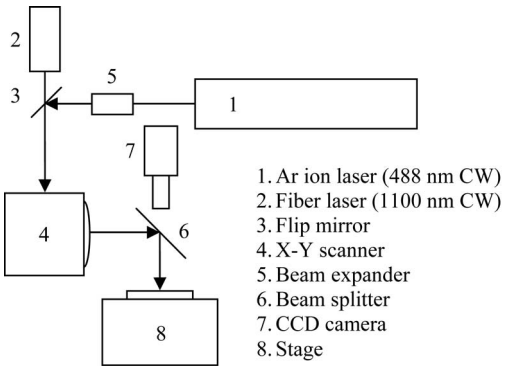

FIG. 1. Schematic of experimental laser sintering setup.

II. EXPERIMENT

Figure 1 shows a schematic of the experimental setup. The entire process takes place in an ambient nonclean room environment. The setup incorporates two continuous wave (cw) lasers which provide the ability to process materials with different optical absorptivities. A 9 W cw fiber laser (JDS Uniphase IFL9) with a wavelength of 1.10 μm was used for all the experiments presented in this work. The beam is focused to a spot size of ~20 μm on the substrate using a lens with a focal length of 165 mm. The optical *x-y* scanner consists of two mirrors each of which is attached to a servomotor. The servomotors as well as the laser on and off are computer controlled so that the laser beam traces a pattern on the substrate. This approach allows the focal point to be moved at speeds greater than 1 m/s without sacrificing precision (<2 μm lateral positioning accuracy). The high speed makes this approach attractive for both rapid-prototyping and higher-volume production. The process is monitored *in situ* with a charge coupled device (CCD) camera which allows alignment of the sample and sintering of multiple layers.

A. Fabrication

DuPont QS300, a commercial silver based thick-film ink, is used in this work. This ink was developed for the conventional screen printing process and has a specified firing temperature of 850 °C. The ink is intended for high temperature substrates such as alumina and normally cannot be processed on glass or polymer substrates because these substrates cannot survive the bulk firing temperatures. Like most conventional thick-film inks, QS300 is a combination of functional particles (submicron silver, platinum, and other conductors), along with glass frit (which serves as a binder) and organic rheological agents adjusted for the screen printing process. The ink has a quoted sheet resistance of 4.5 m$\Omega/\square$ for a 10 μm fired thickness which corresponds to a conductivity σ of 2.22×10^7 S/m or 36% of the conductivity of bulk silver (6.17×10^7 S/m).

The work presented in this paper uses soda-lime glass substrates (standard laboratory microscope slides). Soda-lime glass has a damage threshold of ~550 °C which is about 300 °C lower than the specified firing temperature of QS300. In the experiments, the ink is diluted with thinner (α-terpineol) to lower its viscosity which permits the ink to be applied to the glass substrate. The final wet ink film is 5–10 μm thick after coating. The ink is then dried in a convection oven at a temperature of 150 °C to remove the thinner and any other volatile organic materials. After drying, the ink is sintered by scanning the laser in the pattern to be generated, as shown in Fig. 2. Once the entire pattern has been sintered, the ink that is not sintered is removed using a solvent such as methanol. Other materials can also be patterned on top of previously sintered layers to form structures such as capacitors[7] and resistor networks. Once the final layer is sintered and the unsintered material removed, the pattern is fully functional with no need of additional postprocessing. An example of this functionality is the dc resistance which is measured to characterize its electrical performance.

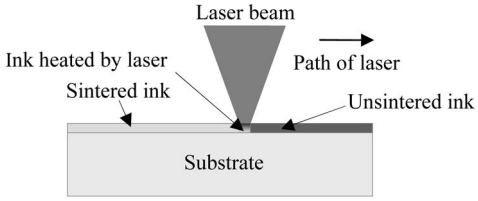

FIG. 2. Laser sintering process.

B. Morphology of laser sintered ink

A parametric study was performed to investigate the effects of the laser processing parameters on the morphology of laser sintered patterns. Lines were created on a 200 μm pitch by moving the laser once over the dried ink. A Tencor Alpha-Step IQ stylus profilometer was used to measure the surface topography. The profiles for several of the sintered lines generated with different laser parameters are shown in Fig. 3. The figure shows that when higher laser powers are used, two bumps form on either side of the centerline traced by the laser. This indicates that where the irradiance of the laser (and thus temperature of the ink) is the highest, the ink is melted and flows laterally due to Marangoni effects.[8] As the intensity of the laser is decreased the amount of melt flow decreases until a continuous line is produced, as shown in Fig. 3(d).

Using the laser focusing condition described previously, further experimentation was able to produce continuous lines with widths less than 25 μm. The height of these lines is close to 1 μm. Figure 4 shows a top view and topographic scans of these lines with a 100 μm pitch. These conductive lines were created by moving the laser across the ink layer at a speed of 0.90 m/s and a power of 1.01 W (measured at the ink surface).

C. dc resistance measurements

The electrical performance of the laser sintered patterns was also investigated using another parametric sweep. Test patterns consisting of a 10×0.425 mm^2 wire between two connectors were written with different laser powers and scan speeds. The larger line width makes the conductors less sensitive to any disparities caused by coating or inconsistencies in the ink. DuPont QS300 ink was again used with soda-lime

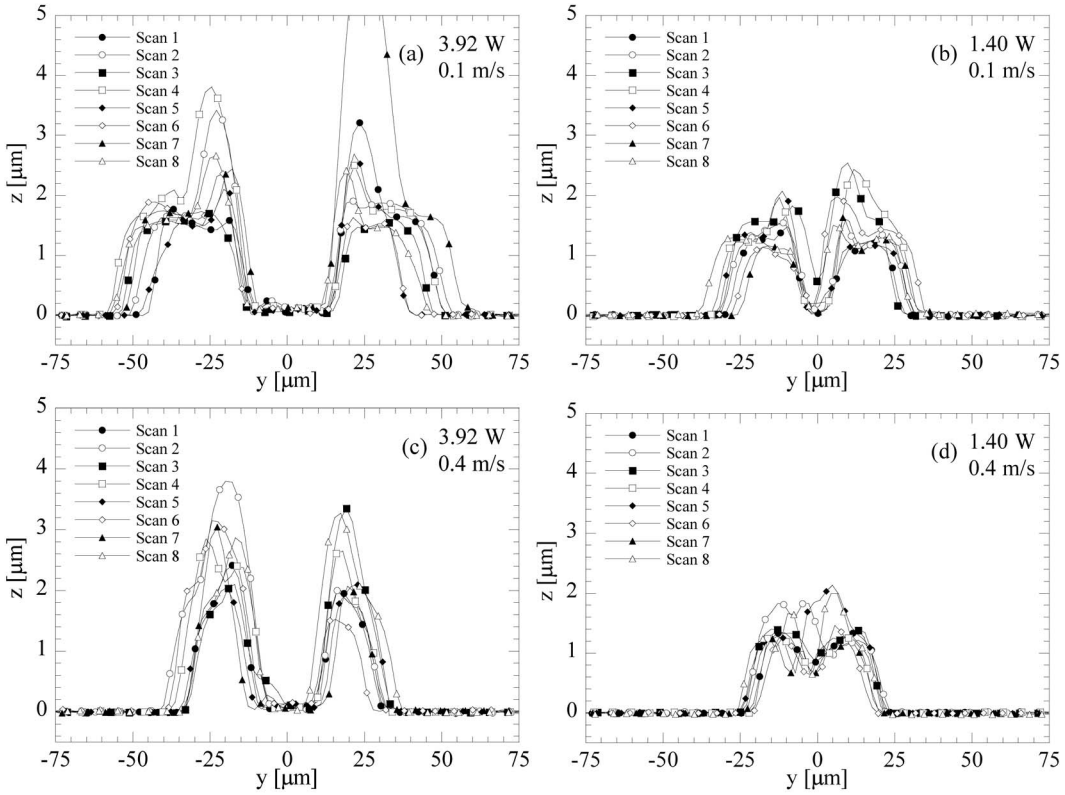

FIG. 3. Single pass lines written at (a) 3.92 W and 0.1 m/s, (b) 1.40 W and 0.1 m/s, (c) 3.92 W and 0.4 m/s, and (d) 1.40 W and 0.4 m/s

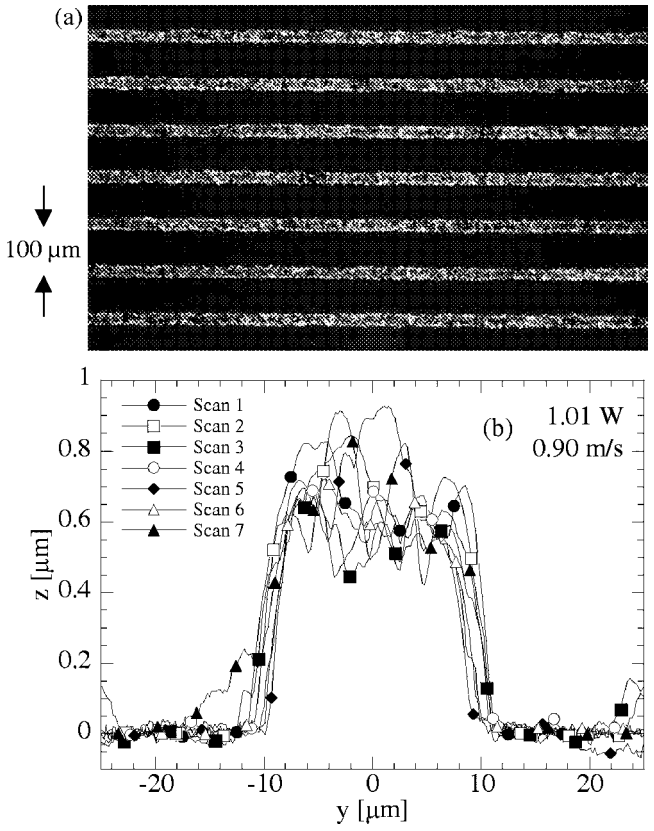

FIG. 4. Photograph (a) and profile (b) of 25 μm wide lines on a 100 μm pitch.

glass substrates. The wires were generated by rastering the laser back and forth with a spacing between the centers of adjacent lines (pitch) of 16 μm. The laser power and scan speed were swept over a range from 0.56 to 3.92 W (measured at the ink surface) and from 0.1 to 1.0 m/s, respectively. Figure 5 shows micrographs of a number of laser-sintered wires. These test patterns all have two layers of sintering. Sintering a second layer helps to fill in voids in the ink, particularly for high power and low speed to overcome coalescence and melting of the pattern. After both the first and second layers were applied the Scotch tape test was conducted and any inadequately bonded material removed.

For low laser powers and high scan speeds the laser energy is insufficient to sinter the ink or bond the ink to the substrate and the parts or whole areas of the pattern are removed during the cleaning step, as shown in Figs. 5(d), 5(g), and 5(h). Within a range of laser powers and scan speeds, the ink is patterned and functionalized, that is, a relatively uniform cross-sectional profile, as shown in Figs. 5(b), 5(e), and 5(i), is produced and the patterns are bonded to the substrate. Finally, for high laser powers and low scan speeds, portions of the ink are totally melted and coalesce to form voids in the pattern. Further, damage to the substrate also occurs as shown in Figs. 5(c) and 5(f). Surface topographies of several of these test patterns are also shown in Fig. 6. Melt reflow and damage to the substrate can be clearly seen at high laser power and slow scan speed. In some of this the increase in volume may be due to permanent structural change in the glass volume very near the interface. This phenomenon is

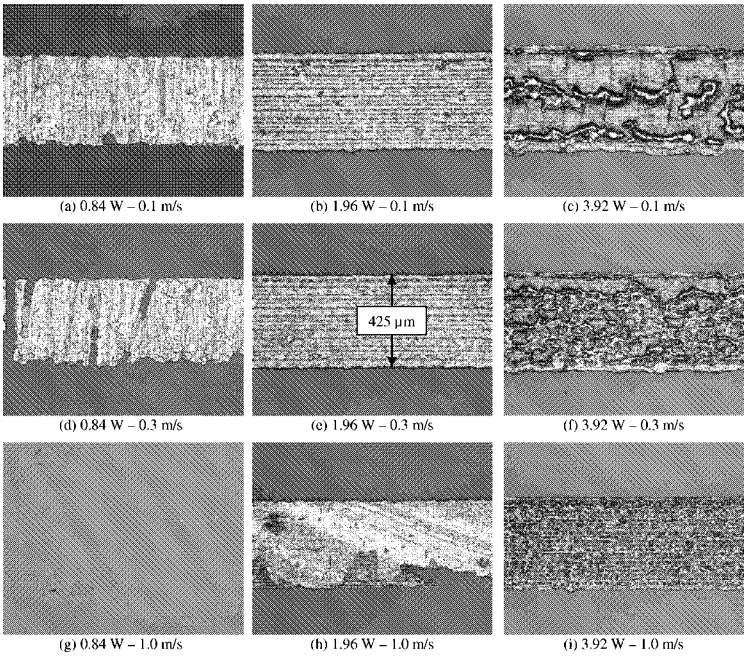

FIG. 5. Micrographs of test patterns written at various speeds and laser powers.

discussed by Shiu *et al.*[9] and occurs when glass is heated above its transition temperature and then cooled very rapidly.

The dc resistance across the sintered pattern was measured using an Agilent 34401A digital multimeter and plotted in Fig. 7. The figure shows that there is a range of laser powers and scan speeds which produce much higher resistance at either too high power/low speed or too low power/high speed. The lowest resistance recorded was 0.355 Ω and occurred for a laser power of 1.96 W and scan speed of 0.1 m/s. The dc conductivity is $\sigma = L/RA$ for a wire with constant cross section, where R is the measured resistance, A is the cross-sectional area, and L is the length of the pattern. The minimum resistance corresponds to a conductivity of 1.97×10^7 S/m, which is obtained with a laser power of 2.24 W and a scan speed of 0.1 m/s, and is 89% of the specified value produced by bulk sintering. However, it should be emphasized again that this ink cannot be conventionally bulk sintered on the soda-lime substrate. Additional improvements to the electrical performance are possible by further refining the laser processing parameters. This includes increasing the laser power for the second and any subsequent layers to take account in the change in the thermal properties of the underlying area. This consideration is particularly true for small features, in which case it is necessary to use less laser energy to generate the pattern, remove the material, and then trace the same pattern a second time with more laser energy to fully functionalize the material. Also the thickness of the ink can also be optimized to produce a more advantageous thermal profile within the ink.

III. THERMAL ANALYSIS

Thick-film inks are designed to be processed at certain temperatures. Therefore, understanding the transient thermal profile during the processing stage is important. The temperature profile for firing thick-film inks, of which QS300 is typical, requires heating the ink to 850 °C at a ramp speed of

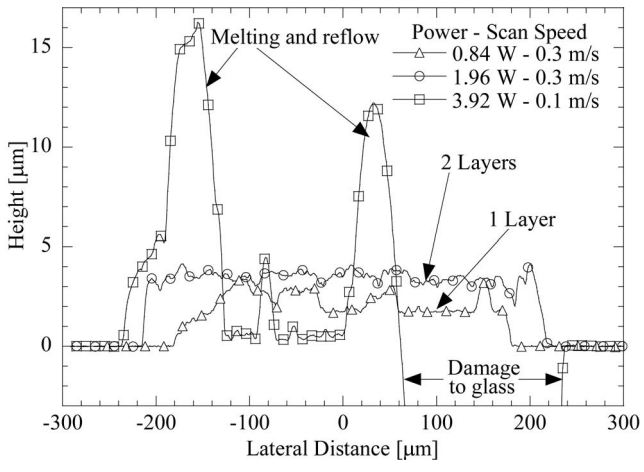

FIG. 6. Cross-sectional profiles of the test patterns in Figs. 5(d), 5(e), and 5(c).

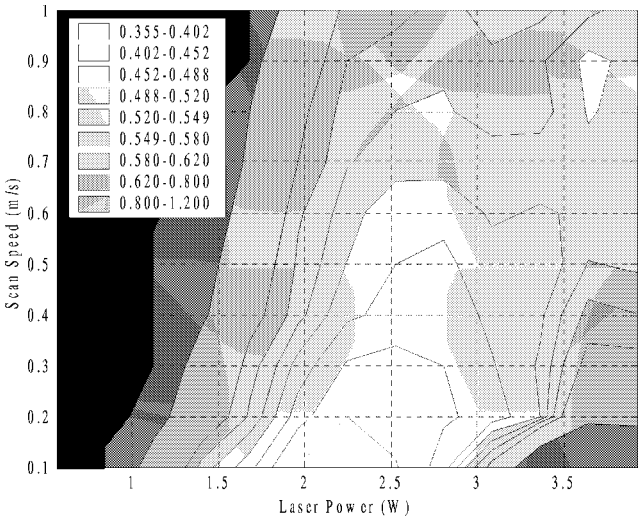

FIG. 7. dc resistance in Ω for 10 mm wire after two layers of metallization.

~50 °C/min, a 10 min dwell at this temperature before cooling back to room temperature at ~50 °C/min.[1] Overall, the typical firing procedure takes about 1 h. In comparison, both the heating and cooling generated by laser sintering are much more rapid with the high temperature at a given point lasting on the order of milliseconds. Also, there is a sharp temperature gradient in the ink during laser sintering, with the temperature at the surface of the ink higher than that at the ink-substrate interface. Such temperature gradients are not present in conventional sintering. Melting of the ink, particularly at the surface, can also occur at higher laser power and/or lower laser scanning speed, as seen in Figs. 3 and 6. Given the nature of thick-film ink sintering, the optimal condition for the laser process is to bring the temperature throughout the ink layer to the sintering temperature (850 °C) while maintaining the substrate temperature as low as possible, with the bulk of the substrate below its damage threshold (~550 °C for soda-lime glasses).

It is difficult to measure the temperature inside the ink and the substrate *in situ*. However, given the material properties and laser parameters, the thermal profile can be computed using numerical simulations. In this work, we use the finite element code ABAQUS (ABAQUS Inc., Providence, RI) to calculate the thermal profile generated in the ink and the substrate for different laser processing parameters and attempt to use the calculation results to explain the experimental data.

The material properties used in the calculations are chosen to represent the ink as close as possible since the exact composition of the ink is proprietary. The ink after drying in the oven and before laser sintering is modeled as a homogenous mixture of 90% silver and 10% soda-lime glass by mass to include the effects of the glass frit. The volatile organic solvents are assumed to be completely driven off during the drying prior to exposure to the laser. The density and specific heat are taken to be the mass-weighted averages of the temperature dependent constituent properties. The effective thermal conductivity is calculated using the Maxwell effective medium theory.[10] This approach is valid for a random suspension of spherical particles in a homogenous medium and gives

$$\frac{k_e}{k_0} = 1 + \frac{3\phi}{[(k_1 + 2k_0)/(k_1 - k_0)] - \phi}, \tag{1}$$

where ϕ is the volume fraction of the spherical inclusions and k_0 and k_1 are the thermal conductivities of the medium and spherical inclusions, in this case the glass frit and the silver particles. It is noted that Maxwell's theory is valid only for low inclusion concentrations and is used here for approximation due to the lack of accurate effective thermal conductivity model at high concentrations. Pure silver has a melting point at 962 °C and a latent heat of fusion of 103 kJ/kg. Glass does not have a classic latent heat and as the glass frit is heated it will experience a glass transition rather than a definitive melting process. Since there is much more silver by mass, the effects of the glass transition are assumed to be negligible. The latent heat of ink is then weighted by the mass fraction of the silver. The effect of melting is considered in the simulation by replacing the specific heat c_p with an effective specific heat $\tilde{c}_p$ that includes latent heat effects,

$$\tilde{c}_p(T) = \begin{cases} c_p(T) & T \leqslant T_s, \quad T \geqslant T_l \\ c_p(T) + \dfrac{h_{fg}}{T_l - T_s} & T_s \leqslant T \leqslant T_l \end{cases}. \tag{2}$$

The latent heat h_{fg} is linearly distributed as an addition to the effective specific heat over a temperature range between T_s and T_l, which can be considered as the solidus temperature for impure materials begin to melt, and the liquidus temperature when melting is completed. The solidus and liquidus temperatures used in this work for the ink are 962 and 1012 °C, respectively. Using an effective specific heat permits the entire ink layer to be treated as a continuous medium modeled by a single domain without calculating the phase boundaries explicitly. The properties of silver are taken from Incropera and Dewit.[11] The properties of soda-lime glass substrate are from Kiyohashi *et al.*[12] and Touloukian.[13] Since the material properties are not precisely known, the numerical results are only intended to capture the trends of the effects of the laser parameters on the thermal profile and are not expected to produce results that definitively correspond to the experiments. The material properties for silver, soda-lime glass, and the simulated ink are plotted in Fig. 8.

The interaction of the laser beam with the ink is modeled as a volumetric heat source moving at a constant velocity. For a laser with Gaussian beam profile, the laser flux at a point (x,y) on the surface of the ink can be expressed as

$$I(x,y,t) = \frac{2P}{\pi r_0^2} \exp\left[-2\frac{(x - x_0 - v_x t)^2 + (y - y_0)^2}{r_0^2} \right], \tag{3}$$

where P is the laser power at the interface, r_0 is the beam radius $(1/e^2)$, v_x is the scan velocity in the x direction, and t is the time.

A portion of the incident laser flux is reflected at the surface while the remainder is absorbed by the ink layer. According to Lambert's law the absorbance produces an exponential attenuation in the incident field. The laser heat flux is then given by

$$q(x,y,z,t) = (1 - R_f) I(x,y,t) \exp(-\alpha z), \tag{4a}$$

where α is the attenuation coefficient and R_f accounts for the surface reflection. The volumetric distribution of the heat source term generated by the absorbed laser energy is given by

$$Q_{\mathrm{ab}} = -\frac{dq}{dz} = \alpha(1 - R_f) I(x,y,t) \exp(-\alpha z). \tag{4b}$$

Both α and R_f are taken as the properties of silver.

The three-dimensional (3D) transient heat conduction equation that governs the heat transfer within the material is

$$\rho c_p \frac{\partial T}{\partial t} = \nabla(k \nabla T) + Q_{\mathrm{ab}}, \tag{5}$$

where c_p is the specific heat, ρ is the density, and k is the thermal conductivity of the medium (either the ink or the substrate). There will be heat transfer via conduction across

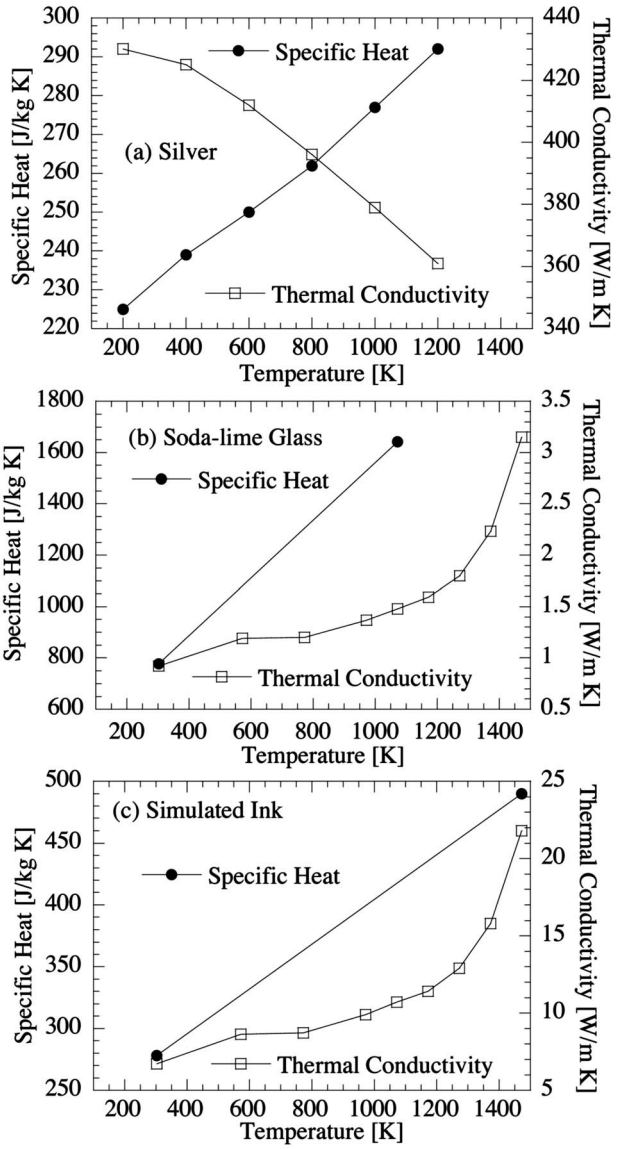

FIG. 8. Specific heat and thermal conductivity for (a) silver, (b) soda-lime glass, and (c) effective values used for simulating ink.

the interface between the substrate and the ink layer. The ink is assumed to completely wet the substrate and the contact resistance is neglected. Because the heat flux leaving the ink must be equal to the heat flux entering the substrate, the thermal profile at the interface is governed by

$$q'' = -k_i \frac{\partial T}{\partial z}\bigg|^{-} = -k_s \frac{\partial T}{\partial z}\bigg|^{+}, \tag{6}$$

where k_i and k_s are the thermal conductivities of the ink and substrate, respectively. The plus and minus signs indicate the side of the discontinuity at the interface.

During the sintering process the ink layer is cooled by convection and radiation exchange with the surroundings. Both convection and radiation are considered at the surface of the ink using Newton's law of cooling for convection with a convection coefficient of 20 $W/m^2 K$ and the Stefan-Boltzmann law with an emissivity of 0.1. However, because

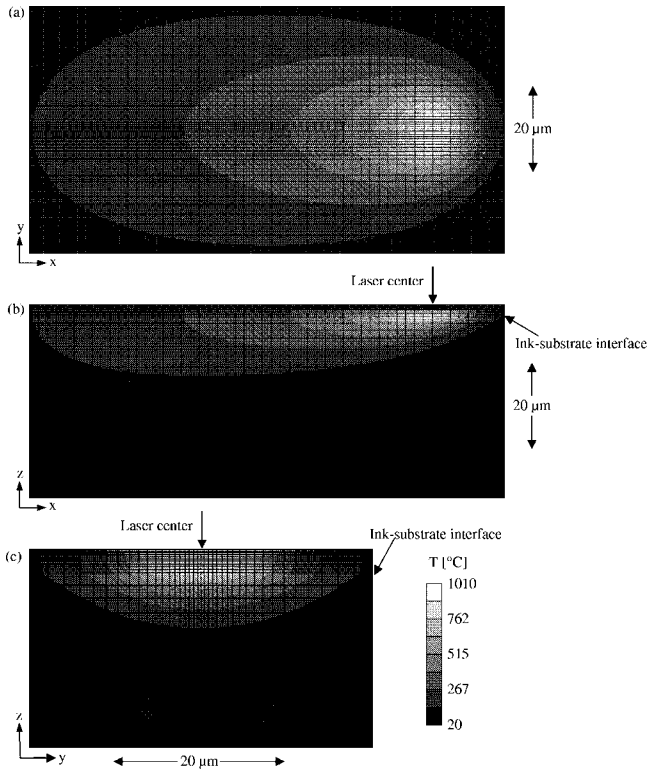

FIG. 9. Thermal profile for a laser power of 2.0 W and a scan speed of 0.10 m/s. (a) Surface xy plane, $z=3$ μm; (b) cross section of central xz plane, $y=0$ μm; and (c) cross section of yz plane, $x=90$ μm.

convection and radiation account for a negligible amount of total heat transfer during laser sintering, the choice of these values proves not to be significant.

The simulation domain is 150 μm wide and 200 μm long. The ink layer and the substrate are 3 amd 75 μm thick, respectively. These two regions share a common set of nodes at the interface. The laser is scanned 100 μm in the x direction along the centerline of the sample starting at 50 μm from the edge. The laser beam is normally incident on the surface of the ink and has a radius r_0 of 10 μm. To reduce the simulation time, the symmetry about the center plane is exploited by assigning an adiabatic boundary condition to this plane. The depth is measured from the interface between the substrate and the ink film ($z=0$) and oriented so that $z=3$ μm corresponds to the surface of the ink. The focal point of the laser starts at $x=0$ μm (50 μm from the edge of the calculation domain) at time $t=0$. It is scanned across the substrate at a constant velocity and finishes 100 μm from the starting point and 50 μm from the opposite edge.

The model uses a total of 99 200 nodes and 92 070 elements. The mesh is uniform along the x direction (the direction along which the laser is scanned) and is more densely spaced in the y and z directions near the laser path where the thermal gradients are higher. In the z direction, the substrate layer has a total of 20 nodes while the ink layer is 12 nodes thick. Both the ink and substrate regions of the mesh are modeled using DC3D8 elements, which are 3D eight-node linear brick elements from the ABAQUS library.

Figure 9 shows results of calculation for a laser power of 2.0 W and a scanning speed of 0.1 m/s, at a time instant

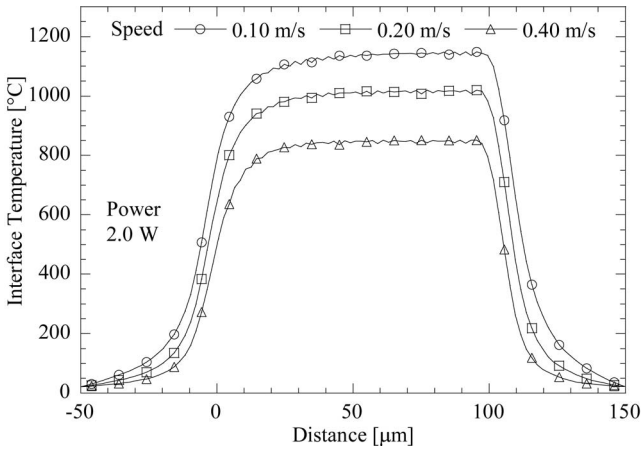

FIG. 10. Maximum temperature attained along the centerline of the ink-substrate interface for 2.0 W of laser power.

when the center of the laser is located 90 μm from the beginning of scan. The figure shows the region of the heated area including the discontinuity of temperature gradient at the interface between the substrate and the ink layer. It is worth pointing out that the depth of thermal penetration into the substrate is confined within several micrometers from the interface.

Because the laser is turned on at the beginning of the scan, the temperature profile takes some time to evolve. Eventually, it does not change with respect to the distance from the starting point. Figure 10 shows the maximum temperatures reached for nodes along the centerline of the interface for a laser power of 2.0 W and different scan speeds. It is observed that when the laser moves faster, the distance required to develop a constant thermal profile is slightly reduced. As shown in the figure, for the three speeds considered, the temperature profile reaches a constant value with respect to distance traveled within 60 μm of the starting point. Knowing the distance for the temperature profile to reach a constant is important for writing microelectronic components with constant properties. In practice, the nonuniformity of the maximum temperature at the beginning of scanning can possibly be overcome by modulating the laser power so that a higher power is applied at the beginning of the scan and then decreases as the thermal profile reaches steady state, or by adding a large contact area such as that used in this work.

From Eq. (6), it is seen that the ratio of the temperature gradients in the ink and substrate is inversely proportional to the ratio of thermal conductivities. The optimum thermal profile for laser sintering on low temperature substrate is to use an ink with high thermal conductivity and a substrate with low thermal conductivity. In this case, the temperature in the ink will tend to be more uniform to prevent damage at the surface of the ink, while the high temperatures in the substrate will be confined to the region near the interface, minimizing the damage to the substrate. At the surface of the ink, the silver particles can be melted because of the temperature gradient in the ink. (Again there is evidence of melting and flow of the ink, as shown in Figs. 3, 5, and 6.) Since the temperature in both media must be equal at the interface,

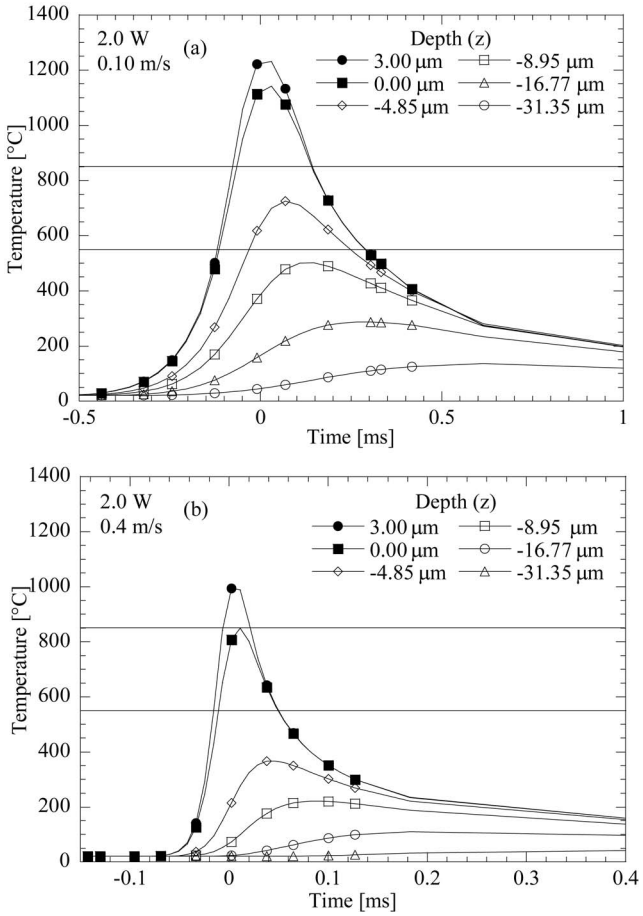

FIG. 11. Transient temperature for a laser power of 2.0 W and scan speeds of (a) 0.10 m/s and (b) 0.40 m/s for several different depths.

at least a portion of the substrate will be heated to the minimum sintering temperature of the ink, meaning the substrate material near the interface is melted if its melting temperature is lower than the sintering temperature. On the other hand, melting a small portion of the substrate may enhance the fusion bonding between the ink and the substrate. These considerations again point to the importance of knowing the thermal profile during laser sintering, which can be obtained from numerical calculations.

Figure 11 shows the transient temperature at different depths inside the ink layer and substrate for a laser power of 2.0 W. $t=0$ corresponds to the instance when the laser center is at the point of consideration at the sample surface ($z=3$ μm), whereas other points are directly underneath the surface point. The location of the surface point does not affect the transient temperature profiles plotted in Fig. 11, as long as it is at a certain distance away from the beginning of scan, as shown in Fig. 10 (>60 μm). The two horizontal lines in the figure indicate the sintering temperature of the ink (850 °C) and the damage temperature of soda-lime glass ($\sim$550 °C). Figure 11 shows that the sintering duration, i.e., the time duration when the ink layer is above the sintering temperature, is only of the order of milliseconds. Also, the substrate near the interface is only above the damage threshold of soda-lime glass for less than 0.5 and 0.2 ms for scan speeds of 0.1 and 0.4 m/s, respectively. The temperature profiles inside the ink and the substrate are better shown in

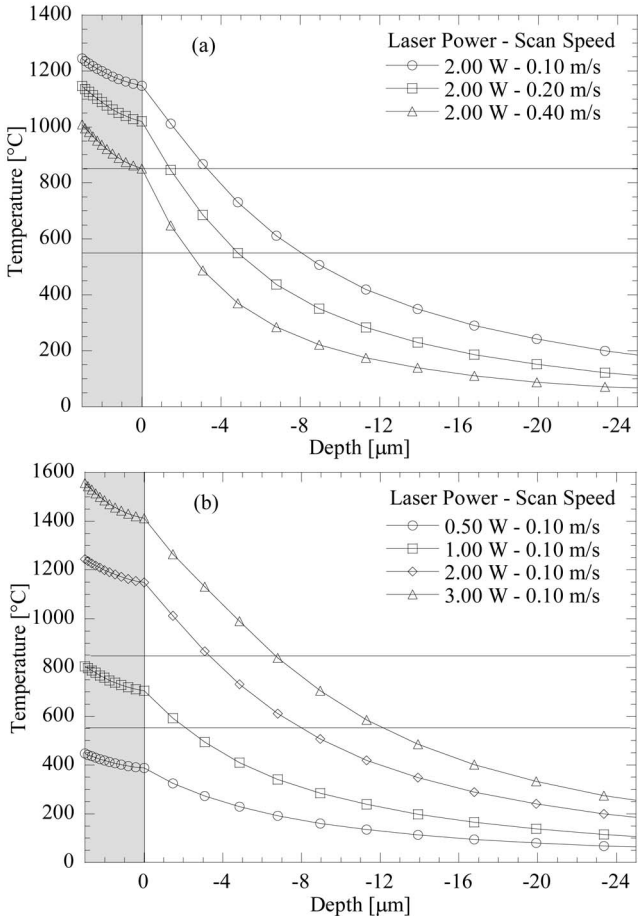

FIG. 12. Maximum thermal profile attained using different scan speeds and powers.

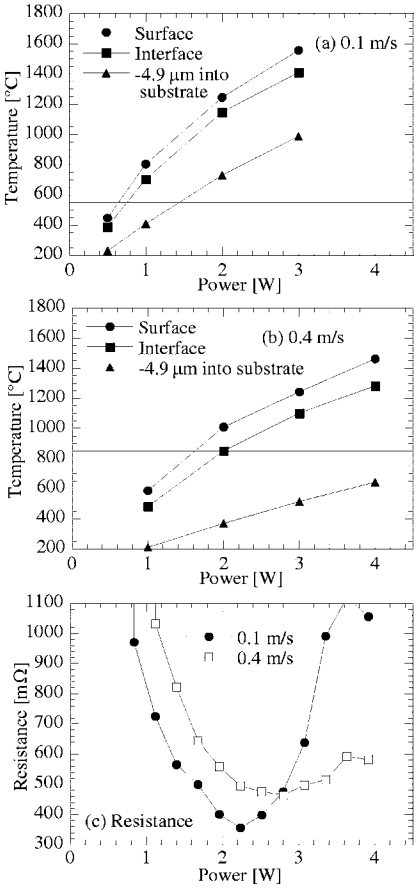

FIG. 13. Comparison between maximum temperatures with dc resistance for different process parameters.

Fig. 12, which plots the maximum temperature attained for different laser scan speeds and different laser powers. Again, the two horizontal lines indicate the sintering temperature of the ink and the damage temperature of soda-lime glass. These temperature profiles show that with the proper selection of the laser parameters (such as with a laser power of 2.0 W and scan speed of 0.10 m/s), the region of the substrate that is heated above its damage threshold can be confined within 4 μm from the interface.

The maximum temperatures attained at the surface of the ink, at the interface between the ink and the substrate, and at 4.9 μm into the substrate are displayed in Fig. 13. Also shown is the dc resistance (extracted from Fig. 7), which decreases with the laser power when the laser power is low. Comparing the dc resistance data with the maximum temperatures at the ink surface and the ink/substrate interface, it is evident that in order to achieve low dc resistance, the entire layer of the ink needs to be heated above the sintering temperature. This requires that the first few micrometers of the glass substrate be heated above the glass transition temperature. This slight overheating appears to contribute to the bonding of the sintered ink to the substrate. At higher laser powers, the ink and the substrate are heated to temperatures well in excess of the melting temperature of the ink and the damage threshold of the glass. The dc conductivity is reduced due to the voids generated in the ink caused by melting along with damage to the substrate. Experimentally, this is shown in Fig. 5, where the ink has melted as well as the substrate, which flows up into the ink. Figures 13(a) and 13(b) also help to explain Fig. 3. It can be seen that the peak temperature clearly exceeds melting point of the ink leading to the lateral flow of the molten material. Limiting this excess peak temperature is a key to improving pattern morphology.

IV. CONCLUSION

In this paper, we investigated the use of laser sintering for the fabrication of thick-film microelectronic components. The technique was demonstrated to be capable of producing patterns with dc conductivity approaching that specified by the manufacture for bulk firing at 850 °C on a substrate that would be unable to withstand the prolonged exposure to these temperatures. Additionally, the approach permits the generation of patterns with smaller feature sizes than what can be conventionally approached without the need for any trimming. A finite element model of the laser sintering process was used to compute the transient temperature profiles. Results of the calculation showed that temperatures above the damage threshold of the substrate can be confined to within a thin layer of a few micrometers. Higher laser power can lead to a lower resistance up to a point when damage occurs due to the melt flow of the ink and the substrate.

ACKNOWLEDGMENTS

The authors wish to gratefully acknowledge the State of Indiana's 21st Century Research and Development Fund for supporting this work. They would also like to thank Carl Berlin at Delphi Delco Electronics Systems for providing the materials and constructive feedback as well as Dr. Richard X. Zhang for assistance with setting up the FEM simulations. One of the authors (E.C.K.) also thanks the Lozar Fellowship of the School of Mechanical Engineering, Purdue University.

[1]J. J. Licari and L. R. Enlow, *Hybrid Microcircuit Technology Handbook*, 2nd ed. (Noyes, Westwood, NJ, 1998).
[2]N. R. Bieri, J. Chung, D. Poulikakos, and C. P. Grigoropoulos, Appl. Phys. A: Mater. Sci. Process. **80**, 1485 (2005).
[3]A. Piqué and D. B. Chrisey, *Direct-Write Technologies for Rapid Prototyping Applications: Sensors, Electronics, and Integrated Power Sources* (Academic, San Diego, 2002).
[4]V. Marinov, J. Microelectronics Packaging 1, 261 (2004).
[5]H. Sigmarsson, E. Kinzel, W. Chappell, and X. Xu, *Antennas and Propagation Society International Symposium*, Washington, DC, 3–8 July 2005 (IEEE, New York,2005), Vol. 1A, pp. 280–283.
[6]E. Kinzel, H. Sigmarsson, X. Xu, and W. Chappell, *35th European Microwave Conference Proceedings*, European Microwave Association, Paris, France, 4–6 October 2005 (IEEE, New York,2005), Vol. 1, pp. 289–292.
[7]H. Sigmarsson, E. Kinzel, W. Chappell, and X. Xu, *Microwave Symposium Digest*, IEEE MTT-S International, San Fransisco, CA, 12–17 June 2006 (IEEE, New York,2006), pp. 1788–1791.
[8]D. A. Willis and X. Xu, J. Heat Transfer **122**, 763 (2000).
[9]T. R. Shiu, C. P. Grigoropoulos, D. G. Cahill, and R. Greif, J. Appl. Phys. **86**, 1311 (1999).
[10]J. C. Maxwell, *Electricity and Magnetism*, 3rd ed. (Clarendon, Oxford, 1904), Pt. II, p. 440.
[11]F. P. Incropera and D. P. Dewitt, *Fundamentals of Heat and Mass Transfer* (Wiley, New York, 2002).
[12]H. Kiyohashi, N. Hayakawa, S. Aratani, and H. Masuda, High Temp. - High Press. **34**, 167 (2002).
[13]Y. S. Touloukian, *Thermophysical of Properties of Matter: Specific Heat of Nonmetallic Solids* (Plenum, New York, 1972), Vol. 5, pp. 1240–1242.